A Parametric Approach to Identify Synergistic Domains of Process Intensification for Reactive Separation

Jianping Li[†] , M.M. Faruque Hasan^{*}

Artie McFerrin Department of Chemical Engineering, Texas A&M University, College Station, TX 77843-3122, USA

Abstract

Process intensification aims to combine multiple tasks within multi-functional units to drastically improve various economic, energy and sustainability metrics of a chemical process. Limited work exists to systematically identify the synergistic domains where intensification outperforms its nonintensified counterparts. In this work, we computationally derive the synergistic domains of reactive separation system. We propose a data-driven approach for multi-parametric programming to approximate the critical regions of nonconvex and nonlinear models. Specifically, we first postulate general models for both intensified and nonintensified systems. We use these models to generate data to train a ReLU-type neural network (NN). The trained ReLU-NN model is formulated as a multi-parametric mixed-integer linear program (mp-MILP), and the critical regions of this mp-MILP define the synergistic feasible domains of intensification. We have derived these synergistic domains of vapor-liquid equilibrium (VLE)-based reactive separation for several industrial applications. These synergistic domains enable quick screening of physical properties that favors intensification.

Keywords: Process Intensification, Multi-parametric Programming, Adaptive Constrained Sampling, Synergy, ReLu Neural Networks

1. Introduction

Process intensification (PI) is a design approach that significantly reduces cost, energy consumption, waste emission, processing volume, and hazards in chemical process [1, 2, 3, 4]. Synergy is one of fundamental principles of process intensification by combining physico-

[†]Current address: Department of Chemical and Biological Engineering and DOE Great Lakes Bioenergy Research Center, University of Wisconsin-Madison, Madison, WI 53706, USA

^{*}Correspondence should be addressed to M.M. Faruque Hasan at hasan@tamu.edu, (979) 862-1449

chemical phenomena in situ [5, 6]. Synergistic effect is a phenomenon that interaction or cooperation of multiple functions in one system to produce a combined effect greater than the sum of their separate effects executed sequentially [5, 7]. Utilizing these synergistic effects has led to many process intensification alternatives such as membrane reactor to shift reaction equilibrium with selective removal of products [8, 9], divided-wall columns with thermal coupling [10], hybrid separation using various driving force [11], mass, work and heat integration [12, 13, 14]. Many other examples appear in the literature of reactive distillation [15, 16, 17]. Among them, production of methyl acetate (MeOAc) from methanol (MeOH) and acidic acid (HOAc) is a well-known example for utilizing synergistic effects among interactive physicochemical phenomena to reduce a production process consisting of 10 equipment into a single reactive extractive distillation column [18, 19].

Due to system trade-offs and thermodynamic bottlenecks, combining physicochemical phenomena in a single equipment may not enhance the system overall performance. For instance, as shown in Li et al. [20] and Lopez-Arenas et al. [21], combing reaction with membrane separation or with vapor-liquid phase equilibrium in situ does not necessarily yield a better system performance than systems that decouple reaction and separation phenomena. Hence, understanding whether combining system components enhances or weakens the individual components is important. Lopez-Arenas et al. points that process intensification is not preferred at minimum driving force [21]. Tian and Pisticoporous identified the envelope of combined reaction and separation system using attainable region [22]. However, limited work exists in systematic interpretation of synergistic conditions to answer the critical question: when intensified systems are favored more than nonintensified systems for certain multi-component systems.

In fact, whether synergistic effects exist depends on defining parameters of the nonintensified or intensified systems. For instance, in the case of reactive distillation, when chemical components in the system varies, thermodynamic property parameters for reaction kinetics and phase equilibrium vary. These parameter variations make reactive distillation configuration a less competitive option compared with partial intensification or vice versa [23]. This feature suggests that for given fixed system structure, as system parameters change, the system components' synergistic effects enhances or weakens. Multi-parametric programming can study parameter's influence on the system performance [24]. The key idea of multi-parametric programming is to identify a mathematical program's explicit optimal solutions as functions of parameters along with the regions of parametric space where these explicit solutions remain optimal [25]. These regions are generally referred as critical

regions (CR). Parametric programming has wide applications including uncertainty analysis [26], model predictive control [27] and multi-objective programming [28]. There exists algorithms or frameworks for exactly solving multi-parametric linear programming (mp-LP), multi-parametric mixed-integer linear programming (mp-MILP) and multi-parametric mixed-integer quadratic programming (mp-MIQP) [29]. The solution of multi-parametric nonconvex nonlinear programming (mp-NLP) and multi-parametric mixed-integer nonconvex nonlinear programming (mp-MINLP) is generally approximated through relaxation of nonconvex terms using convex underestimators and overestimators, and developing solution strategy using branch-and-bound or decomposition [25]. Solution of multi-parametric programming problem becomes even more challenging when parameter appears as left-hand parameters, forming bilinear terms between parametric space and variable space. Approximate solution of multi-parametric programming with bilinear terms and left-hand side parameters can follow relaxation of bilinear terms using MaCormick Relaxation, and overlapping evaluation of critical regions [30]. This class of algorithm can yield many CRs.

In this work, we develop general models with common model building blocks for non-intensified (NPI) and intensified (PI) systems along with their unique conditions. These models are formulated as mp-NLP. We adaptively generate samples with input on system parameters and output as driving force difference of NPI and PI, and train neural networks. These neural networks are exactly reformulated as mp-MILP when the activation function is ReLu function. The mp-MILP are solved to obtain explicit expression of optimizer and the corresponding critical regions. These solutions are used to describe feasible and synergistic domains. The technical flow of this work is summarized in Figure 1. In summary, the main contributions of this work include:

- A modeling method for nonintensified and intensified systems with common model building blocks and their unique conditions,
- A data-driven approximate algorithm for multi-parametric nonlinear programming,
- An explicit interpretation of feasibility and synergistic domains of nonintensified and intensified system using parametric programming.

The remainder of the article is structured as follows. First, we describe systems of interest using pairs of physicochemical phenomena and formalize the problem statement. Then, we describe the mp-NLP models for nonintensified and intensified systems with component property parameters. Next, we present an approximate algorithm for solving mp-NLP

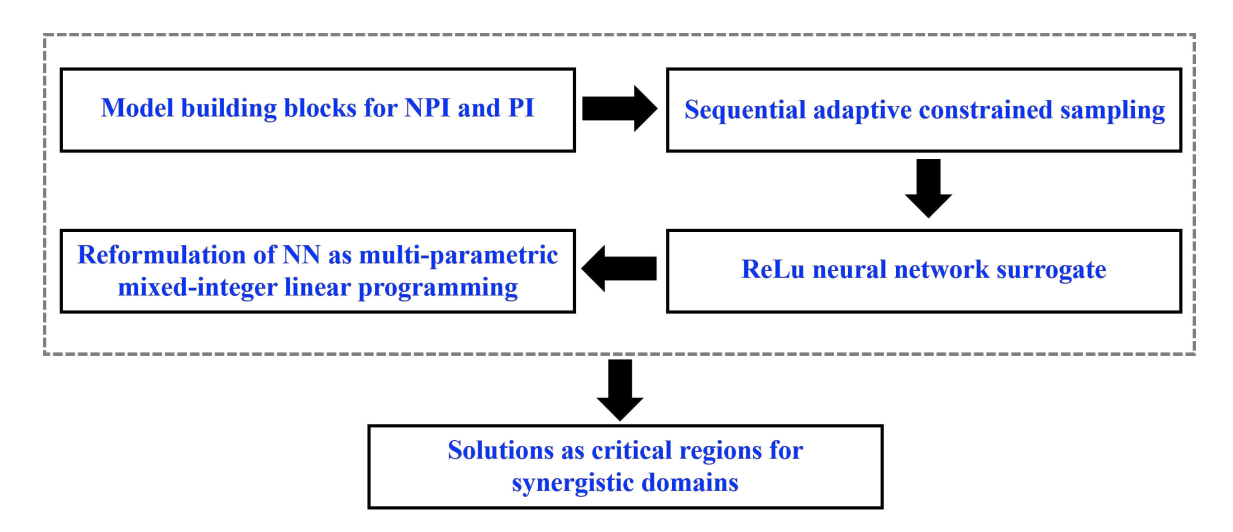


Figure 1: Framework of exploring synergistic domains of intensification using parametric programming. Model building blocks of nonintensification (NPI) and intensification (PI) generate data. Sequential adaptive constrained sampling explores model feasible space and connects with neural network surrogate. The neural network with ReLu activation function is reformulated as multi-parametric mixed-integer linear programming problem (mp-MILP) and solved as critical regions for describing synergistic domains of intensification.

problems. Finally, we demonstrate the applicability of our models and algorithms on several case studies with industrial applications.

2. Systems of Interest and Problem Statement

Many interactions exist among physicochemical phenomena to achieve synergistic process intensification. These interactions can be classified into reaction-separation phenomena interactions and separation-separation phenomena interactions. Synergy between reaction and separation operations is common in chemical operations. To simplify the discussion, we focus on systems involving equilibrium-based reactions which is followed by a vapor-liquid separation operation for product enrichment. Reaction equilibrium at specified reaction conditions represents the maximum conversion attainable. Phase equilibrium determines an upper limit for mass transfer. The methodology presented in this work is general for investigating synergistic effects of other phenomena-phenomena interactions. The nomenclature is given in the Supporting Information. This section firstly describes the systems of interest, existence of potential synergy and then demonstrates the problem statement.

System descriptions are given in Figure 2. Both systems involve I components $(i = \{1, ..., I\})$, N reactions $(n = \{1, ..., N\})$ and a common feed stream with total flowrate F^0

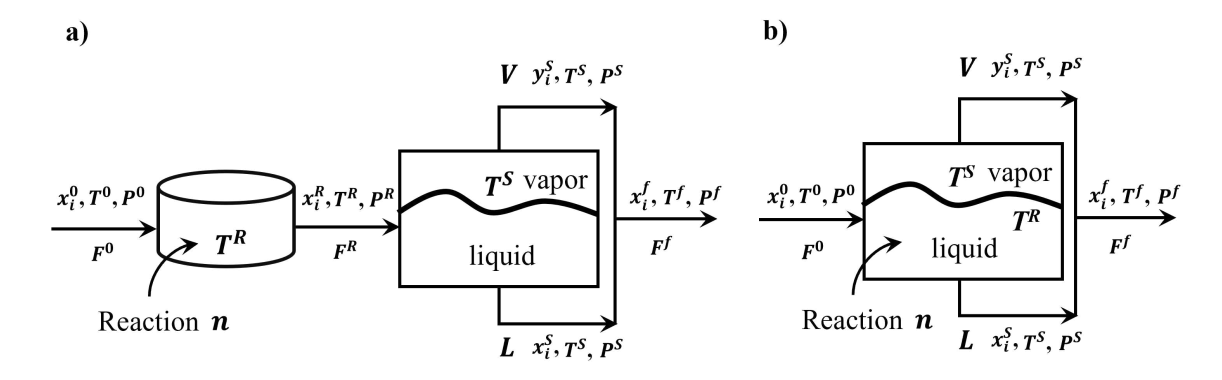


Figure 2: Process flowsheets for nonintensified and intensified reaction-separation systems. a) Nonintensified system with reaction followed by separator and b) Intensified system with reaction and separation in situ.

and state tuple (x_i^0, T^0, P^0) in composition x, temperature T and pressure P respectively. Nonintensified system (NPI) involves a single-phase reactor (R) followed by a separator (S). The feed stream with total flowrate F^0 enters the reactor with reactions n in liquid phase, which changes initial feed compositions or yield new component in reactor outlet stream. The state of this reactor outlet stream with total flowrate F^R is (x_i^R, T^R, P^R) . The reactor outlet is fed into separator operated at temperature T^S . The outlet stream of this separator involves a vapor stream with total flow rate V and state $(y_i^S,\,T^S,\,P^S)$ and a liquid stream with total flow rate L and state (x_i^S, T^S, P^S) . y_i^S is the vapor composition of component i. Intensfied system (PI) combines reaction and vapor-liquid phase equilibrium in a single unit. The same feed stream with total flowrate F^0 and state (x_i^0, T^0, P^0) is converted into a vapor stream with flow rate V and state (y_i^S, T^S, P^S) and a liquid stream with flow rate L and state (x_i^S, T^S, P^S) . The separation (reaction) is operated at temperature T^S (T^R) and pressure P^S (P^R) respectively. For modeling and analysis convenience, the vapor (V) outlet and liquid (L) outlet of nonintensified and intensified system are mixed as a stream with total flow rate F^f and state (x_i^f, T^f, P^f) . Variable x_i^f, T^f and P^f are composition, temperature and pressure of this stream respectively. The state (x_i^f, T^f, P^f) is also a pseudo inlet state to phase equilibrium in nonintensification.

Property parameters defining given systems are θ^R for reaction equilibrium, and θ^S for vapor-liquid equilibrium. θ^R and θ^S are uniquely defined for each system and independent of state in composition, temperature and pressure. Parameter matrix θ^S involves parameters $\theta_i^{S,sat}$ for component saturated pressure using Antoine equations and parameters $\theta^{S,act}$ for activity coefficient calculation. The is denoted as $\theta^S = (\theta_i^{S,sat}, \theta^{S,act})$. If the Antoine equation

is $P_i^{sat} = exp(A_i + \frac{B_i}{(C_i + T)})$, then $\theta_i^{sat} = (A_i, B_i, C_i)$. The number of θ^R and $\theta^{S,act}$ defining the system depends on the number of components and thermodynamic models used. For instance, for a system involving I number of components, if we consider Wilson model for determining activity coefficient in liquid phase, then we have $\frac{I(I+1)}{2} + I$ number of parameters [31]. If we consider UNIQUAC model for liquid phase activity coefficient, then we have $\frac{I(I+1)}{2} + 2I$ number of parameters [31]. The activity coefficient models and the procedure of counting the number of parameters are given in the Supporting Information.

If the reaction is exothermic, then increasing T^R is not favorable for reaction conversion according to Le Chatelier's principle. For intensified systems (PI), in situ removal of reaction product helps to shift reaction equilibrium to product side. Hence, when separation in the system becomes easier, the reaction conversion for PI is higher. However, PI system only involves one temperature $T^S = T^R$. When reaction is more exothermic, the system favors low temperature for product yield while favors high temperature for product purity enrichment. In this case, nonintensified system with reaction followed by separation becomes favorable. Transition regions on parameters defining reaction and separation exist such that PI outperforms NPI or vice versa. The problem statement is as follows: Given set of component $(i = \{1, ..., I\})$ and set of reaction $(n = \{1, ..., N\})$ in the system, find domains on system parameters $\theta \in \Theta$ that enables PI system gives better process performance than NPI system or vice versa. We refer parametric domains when PI yields better process performance than NPI as synergistic domains. These type of problems can be formulated as multi-parametric programming or handled with sensitivity analysis.

3. Mathematical Models

In this section, we present the mathematical models for intensified and noninensified systems respectively. Firstly, we present the rigorous models for these two systems using equilibrium-based reaction and phase equilibrium models. These two systems are described using common model building blocks and their unique conditions on compositions, temperature and pressure. Next, we impose assumptions to simplify the proposed rigorous models to reduce the number of property parameters without compromising necessary system information. The objective function is to maximize system driving force. Finally, we present the simplified models of intensified and nonintensified systems. These simplified models enable the sample generation for data-driven multi-parametric programming in Section 4.

3.1. Rigorous Models

Based on flowsheet description of nonintensified and intensified system in Section 2, we describe the common constraints (CC) for nonintensified and intensified systems as follows:

$$K_n^R = \prod_i (\gamma_i^R x_i^R)^{\nu_{n,i}}$$
 $\forall n \in \mathbb{N}$ (1)

$$\gamma_i^R = f(x_i^R, T^R, \theta^R) \qquad \forall i \in I \ (2)$$

$$K_n^R = exp(-\frac{\Delta G_n^{rxn}}{RT^R}) \qquad \forall n \in N \ (3)$$

$$F_0 x_i^0 + \sum_{n} \xi_{n,k} \nu_{n,i} = F^f x_i^f \qquad \forall i \in I \quad (4)$$

$$F^f x_i^f = V y_i^S + L x_i^S$$
 $\forall i \in I$ (5)

$$K_i^S = P_i^{sat}(T^S, \theta_i^{sat}) \gamma_i^S(x_i^S, T^S, \theta^{S, act}) / P^S$$
 $\forall i \in I \ (6)$

$$y_i^S = K_i^S x_i^S$$
 $\forall i \in I$ (7)

$$\sum_{i} x_i^S = 1, \quad \sum_{i} y_i^S = 1, \quad \sum_{i} x_i^f = 1$$
 (8)

CC represents Eqs. 1–8. Eq. 1 defines the equilibrium constant of reaction n using activity coefficient γ_i^R of component i and reaction outlet composition x_i^R along with the component stoichiometric coefficient $\nu_{n,i}$ of reaction n. Note the convention that the stoichiometric coefficients are negative for reactants and positive for products. Eq. 2 determines the liquid phase activity coefficient γ_i^R using activity coefficient models, e.g., Wilson models and UNIQUAC. Here, we only consider liquid-phase reactions covering a wide range of important reactions. Gas-phase reactions can be incorporated by revising the expression of reaction equilibrium constant K_n^R (Eq. 3) using vapor composition and fugacity coefficients of components involved in reactions. Eq. 3 determines the reaction equilibrium constant using Gibbs energy of reaction ΔG^{rxn} and reaction temperature T^R (adapted from equilibrium reaction model from Seider et al. [32]). Eq. 4 is molar balance for the whole system (nonintensified or intensified). F_0 and F^f are total inlet flow and outlet flow of systems. x_i^0 and x_i^f defines the inlet and outlet composition of systems. $\xi_{n,k}$ is the extent of reaction n for key reactant $k \in I$ with stoichiometric coefficient as $\nu_{n,k} = -1$. Eq. 5 indicates that the outlet flow is the mixture of vapor flow V and liquid flow L from the flash operation. The composition for vapor flow and liquid flow are \boldsymbol{x}_i^S and \boldsymbol{y}_i^S respectively.

Eq. 6 determines the phase equilibrium constant K_i^S for component i. Here, $P_i^{sat}(T^S, \theta_i^{sat})$ is the saturated pressure, which is a function of separator temperature T^S . $\gamma_i^S(x_i^S, T^S, \theta^{S,act})$ is the activity coefficient of component i in the liquid phase. P^S is the separator pressure.

Ideal gas condition in vapor phase is assumed and hence fugacity coefficient is equal to one. Eq. 7 defines equilibrium relation between liquid and vapor composition. Eq. 8 indicates that summation of composition fractions goes to one. The alternative models using kinetics-based reactions can be found in Li [33]. In addition to these common constraints that describe the nonintensified and intensified systems, another two set of unique conditions (denoted as NPI-C and PI-C) exist that indicate the physical conditions of nonintensification and intensification respectively. In another words, nonintensified system is described through CC + NPI-C and intensified system is described through CC + NPI-C.

$$x_i^R = x_i^f, \ T^R \le T^{BUB}(x_i^f, P^f), \ T^S \le T^{DEW}(x_i^f, P^f)$$
 (NPI-C) (9)

$$x_i^R = x_i^S, \ T^R \ge T^{BUB}(x_i^f, P^f), \ T^S \le T^{DEW}(x_i^f, P^f), \ T^R = T^S, \ P^R = P^S$$
 (PI-C) (10)

NPI-C indicates that in the case of nonintensification, the reaction outlet composition is equal to that of system outlet composition. Besides, reaction temperature is below the bubble point if the reaction happens in liquid phase. And separation temperature is below the dew point. Here both bubble and dew points are dependent on the state of final outlet stream due to the equivalence of reaction outlet and system outlet. NPI conditions on reaction temperature T^R can be revised to $T^R \geq T^{DEW}(x_i^f, P^f)$ if the reaction occurs in vapor phase. T^{BUB} and T^{DEW} refer to bubble point and dew point temperature respectively, which are function of pseudo inlet state (x_i^f, P^f) for composition and pressure. PI-C indicates that for intensified system, the reaction outlet composition is equal to that of separation liquid outlet and the reaction temperature (pressure) equals to separation temperature (pressure). Energy balance is not included here as the energy balance can be satisfied with sufficient amount of utility investment and hence will be redundant. In fact, the model equations for intensified system (CC+PI-C) can be reformulated to keep one liquid phase composition $(x_i^R \text{ or } x_i^S)$ and operation temperature $(T^R \text{ or } T^S)$. This reformulated model is equivalent to other model formulations for intensified systems, such as the work of Sanderson and Chien [34], Barbosa and Doherty [35]. NPI-C and PI-C conditions also indicate that $T^{DEW}(x_i^f, P^f) \geq T^{BUB}(x_i^f, P^f)$. It can be shown that if the system pressures (P^R) and P^{S}) are fixed as constant and one reaction exists, then nonintensified system involves two degree of freedom $(T^R \text{ and } T^S)$ and intensified system involve one degree of freedom, i.e., operating temperature [36]. The degree of freedom is denoted as DOF.

3.2. Model Simplification

The proposed model involves many system parameters and nonlinear terms in molar balances, reaction and phase equilibrium. We impose the following assumptions to simplify the modeling of reaction and phase equilibrium while not compromising important property parameters defining the physical systems.

Assumption 1: we assume that K_n^R can be directly related with $\prod_i (x_i^R)^{\nu_{n,i}}$. Hence, the equilibrium constant is composition-based instead of activity-based. This composition-based equilibrium constant is denoted as $K_n^{R,x}$. The equilibrium constant can be calculated and related with reaction temperature T^R as follows:

$$K_n^{R,x} = \prod_{i} (x_i^R)^{\nu_{n,i}}$$
 $n \in N$ (11)

$$K_n^{R,x} = exp(A_n + \frac{B_n}{T^R})$$
 $n \in \mathbb{N}$ (12)

Eq. 11 – 12 essentially fit integration of van't Hoff equation $(\frac{dlnK}{dT})_p = \frac{\Delta H^{rxn}}{RT^2}$ when ΔH^{rxn} is independent of temperature within certain temperature ranges [32]. Here A_n and B_n are system parameters define reaction equilibrium of reaction n. $A_n = lnK_n^0$ corresponds with $lnK_n^{R,x}$ at reference sates. Hence, when lnK_n^0 are the same for multiple reactions at the different reference states, A_n can be fixed as a common value to reduce the number of parameter input. B_n is $\Delta G_n^{rxn}/R$ (Gibbs energy of reaction at the reference state) or $\Delta H_n^{rxn}/R$ (heat of reaction at the reference state) depending on data availability. Using Eq. 11 – 12 to replace Eq. 1 – 3, we avoid all parameters involved with liquid-phase activity coefficient calculation.

Assumption 2: we assume that K_i^S can be expressed as a linear function of phase equilibrium temperature in the following form (Figure 3):

$$K_i^S = m_i^S T^S + b_i^S$$
 $i \in I$ (13)

Using Eq. 13 to replace Eq. 6, we avoid all parameters involved with saturated pressure, activity coefficient and fugacity coefficient. m_i^S and b_i^S are slopes and intercepts of these linear relations for component i. Both m_i^S and n_i^S take into account the influence of composition and temperature on phase equilibrium and characterize phase equilibrium performance. Besides, relative volatility $\alpha_{i,i'}$ between component i and i' is the ratio of K_i^S and $K_{i'}^S$. The following equation shows that relative volatility between two components can be determined using m_i^S if $b_i^S = 0$:

$$\alpha_{i,i'} = \frac{m_i^S T^S}{m_{i'}^S T^S} = \frac{m_i^S}{m_{i'}^S} \qquad i \in I, i' \in I \quad (14)$$

The approximation of phase equilibrium using linear relation within narrow temperature range is more accurate. As shown in Figure 3, around the reference phase equilibrium point $(T^{S,\Delta},K^{S,\Delta})$, the predicted equilibrium constant using Eq. 13 is the same as actual equilibrium constant at this point. For wider temperature range, Eq. 13 is a linear regression within that range and captures the overall behavior of phase equilibrium. This observation suggests that if m_i^S varies with temperature, then the linear approximation at desired temperature can be improved. Similar to reaction equilibrium, we fix b_i^S as constant for multiple components to reduce parametric inputs. Besides, within narrow range of reaction composition change in liquid phase, we consider the bubble/dew points $T^{BUB}(x_i^f, P^f)/T^{DEW}(x_i^f, P^f)$ as constant parameters, e.g., $T^{BUB}(x_i^f, P^f) = T^{BUB}$.

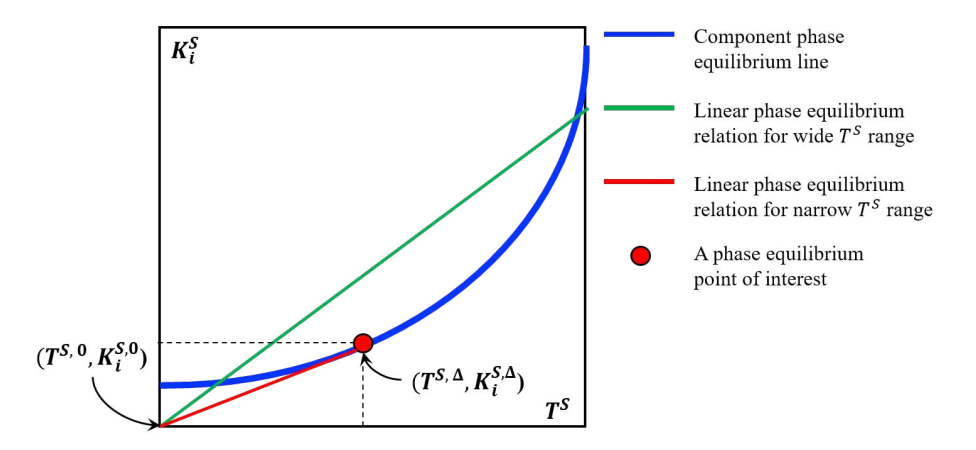


Figure 3: An illustration of linear approximation of phase equilibrium. At the phase equilibrium point of interest, the linear approximation is exact. For wider temperature range, the linear approximation captures overall phase equilibrium feature.

.

We use $\theta^{CC} = (B_n, m_i^S)$ for parameters involved with common constraints and $\theta^{UC} = \{T^{BUB}, T^{DEW}\}$ for parameters involved with unique conditions. We denote the common constraints for nonintensified and intensified systems under simplifying assumptions as CC-S (involving Eqs. 11 – 12, 4 – 5, 13, 7 – 8). CC-S can be copied into CC-S^{NPI} and CC-S^{PI} to distinguish nonintensified and intensified systems respectively. Using DOF of CC-S, the following relations are held:

$$CC-S^{NPI} = f^{NPI}(T^{R,NPI}, T^{S,NPI}, \theta^{CC})$$

$$(15a)$$

$$CC-S^{PI} = f^{PI}(T^{R,PI}, T^{S,PI}, \theta^{CC})$$

$$(15b)$$

Similarly, the unique conditions in Eqs. 9-10 for nonintensified and intensified systems

can be summarized as follows:

$$(x_i^{R,NPI}, x_i^{f,NPI}, T^{R,NPI}, \theta^{UC}) \in \pi^{\text{NPI-C}}$$
(16a)

$$(x_i^{R,PI}, x_i^{S,PI}, T^{R,PI}, \theta^{UC}) \in \pi^{\text{PI-C}}$$

$$(16b)$$

 $\pi^{\text{NPI-C}}$ is a set defined on composition and temperature using unique conditions (shown in Eq. 9) of nonintensified sytems. $\pi^{\text{PI-C}}$ is a set defined on composition, temperature and pressure using unique conditions (shown in Eq. 10) of intensified sytems. The vector for all system parameters is denoted as $\theta = (\theta^{CC}, \theta^{UC}) = (B_n, m_i^S, T^{BUB}, T^{DEW})$. Hence, there are N + I + 2 number of parameters defining nonintensified and intensified systems under simplifying assumptions.

3.3. Objective Function

In this work, we choose the driving force as performance metric [21]. This driving force is the absolute difference of product purity (for product component $i^* \in I$) in vapor phase and liquid phase at phase equilibrium. This objective function can be formulated as follows for nonintensified and intensified systems respectively:

$$obj^{NPI} = |y_{i*}^{S,NPI} - x_{i*}^{S,NPI}| \tag{17}$$

$$obj^{PI} = |y_{i^*}^{S,PI} - x_{i^*}^{S,PI}| \tag{18}$$

3.4. mp-NLP Models for Nonintensified and Intensified Systems

Under simplifying assumptions listed in Section 3.2, we now describe the mp-NLP formulations for nonintensified and intensified systems. Both of these two models involve common constraints CC-S, their unique conditions (NPI-C or PI-C) and system parameters θ . These two problems for nonintensified and intensified systems are denoted as mp-NLP^{NPI} and mp-NLP^{PI} respectively and presented as follows:

$$\begin{aligned} \text{(mp-NLP}^{NPI}) & \begin{cases} \max & obj^{NPI}(\theta) = |y_{i^*}^{S,NPI} - x_{i^*}^{S,NPI}| \\ \text{s.t.} & \text{CC-S}^{NPI} = f^{NPI}(T_i^{R,NPI}, T_i^{S,NPI}, \theta^{CC}) \\ & (x_i^{R,NPI}, x_i^{f,NPI}, T^{R,NPI}, \theta^{UC}) \in \pi^{\text{NPI-C}}, \theta = (\theta^{CC}, \theta^{UC}) \in \Theta \subseteq R^{n_{\theta}} \end{aligned}$$

$$\begin{aligned} \text{(mp-NLP}^{PI}) & \begin{cases} \max & obj^{PI}(\theta) = |y_{i^*}^{S,PI} - x_{i^*}^{S,PI}| \\ \text{s.t.} & \text{CC-S}^{PI} = f^{PI}(T_i^{R,PI}, T_i^{S,PI}, \theta^{CC}) \\ & (x_i^{R,PI}, x_i^{S,PI}, T^{R,PI}, \theta^{UC}) \in \pi^{\text{PI-C}}, \theta = (\theta^{CC}, \theta^{UC}) \in \Theta \subseteq R^{n_{\theta}} \end{aligned}$$

 θ is the vector of system parameters and belongs to the bounded set Θ with the dimension as the number of parameters n_{θ} . The detailed models of mp-NLP^{NPI} and mp-NLP^{PI} are given in the Supporting Information.

3.5. Definition of Synergistic Effects using Optimality

It is desired to operate the chemical system under optimal operating conditions. The change of systems' driving force with their DOF is shown in Figure 4. As mentioned in Section 3.1, nonintensified systems involve two DOF as $T^{R,NPI}$ and $T^{S,NPI}$ under constant operating pressure. Intensified systems involve one DOF as $T^{R,PI} = T^{S,PI}$ under constant operating pressure. As magnitude of DOF in the system varies, the driving force of the system fluctuates. Generally, this type of relation is highly nonlinear and nonconvex considering the nonlinear functions used to describe the model physics.

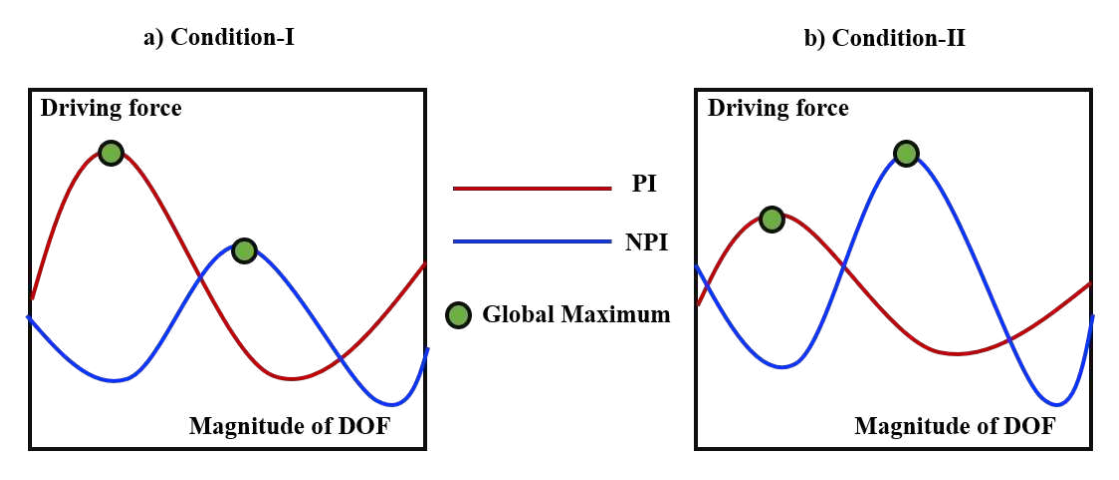


Figure 4: An illustration on the change of system driving force synergy with the magnitude of degree of freedom. a) Condition-I: maximum driving force of PI is larger than maximum driving force of NPI (PI is preferred), and b) Condition-II: maximum driving force of NPI is larger than maximum driving force of PI (NPI is preferred).

•

By running the mp-NLP^{NPI} and mp-NLP^{PI} optimization models respectively, we obtain the operating conditions on reaction and separation temperature under the maximum driving force for NPI and PI system. These maximum driving forces are denoted as $obj^{NPI,*} = |y_{i^*}^{S,NPI} - x_{i^*}^{S,NPI}|^{max,*}$ and $obj^{PI,*} = |y_{i^*}^{S,PI} - x_{i^*}^{S,PI}|^{max,*}$ for NPI and PI. If $obj^{PI,*} \geq obj^{NPI,*}$, then PI can achieve higher driving force compared with NPI under optimal conditions. In this case, PI outperforms NPI due to PI's synergistic effects. If

 $obj^{PI,*} \leq obj^{NPI,*}$, then NPI can achieve higher driving force compared with PI under optimal conditions. The designer should choose NPI system to operate instead of PI system. These relations are summarized as follows:

$$|y_{i^*}^{S,PI} - x_{i^*}^{S,PI}|^{max,*} \ge |y_{i^*}^{S,NPI} - x_{i^*}^{S,NPI}|^{max,*}$$
 (PI is prefered) (19)

$$|y_{i^*}^{S,NPI} - x_{i^*}^{S,NPI}|^{max,*} \ge |y_{i^*}^{S,PI} - x_{i^*}^{S,PI}|^{max,*}$$
 (NPI is prefered) (20)

The above two relations suggest that given system parameters θ , if we evaluate the objective value difference of nonintensified systems and intensified systems, i.e., $obj^{NPI,*}(\theta) - obj^{PI,*}(\theta)$, then we know which system is preferred. Hence, $obj^{NPI,*}(\theta) - obj^{PI,*}(\theta)$ is an important output indicator for given input parameter vector θ .

4. Data-driven Multi-Parametric Programming

The multi-parametric nonlinear programming formulations for nonintensified and intensified systems are denoted as mp-NLP^{NPI} and mp-NLP^{PI} respectively. The involved parameters define reaction and phase equilibrium under simplifying assumptions. These parameters are left-hand parameters that form bilinear terms between variable space and parametric space (e.g., m_i^s) or parameters involved in the remaining reaction nonlinear terms (e.g., B_n). In addition, the existence of many bilinear terms in molar balances makes the exact solution of mp-NLP^{NPI} and mp-NLP^{PI} computationally expensive. Hence, we develop an approximate algorithm to solve these mp-NLPs.

This algorithm is illustrated in Figure 5. We use a constrained sampling problem (the formulation is the same as the one given in Section 4.1) to generate initial samples (e.g., 150 samples). The input system parameters are scaled within [0,1]. Then we use neural network (NN) as surrogate to obtain the relation between input parameters and output objective value difference. The details of neural network formulation are given in the Supporting Information. This surrogate is iteratively evaluated using test samples generated from adaptive constrained sampling (Section 4.1). Around the data region with maximum errors, new samples are inserted. This procedure helps to avoid overfitting, identify data errors and generate enough training samples. When current sample size (NP) is larger than threshold sample size (NC), validations using random samples initialize. When termination criterion (e.g., coefficient of determination R^2 is greater than a threshold value R^0) is met, the output data together with validation data is used to train a simpler neural network with ReLu activation function. This neural network is reformulated as a multi-parametric mixed-integer linear programming problem (Section 4.2).

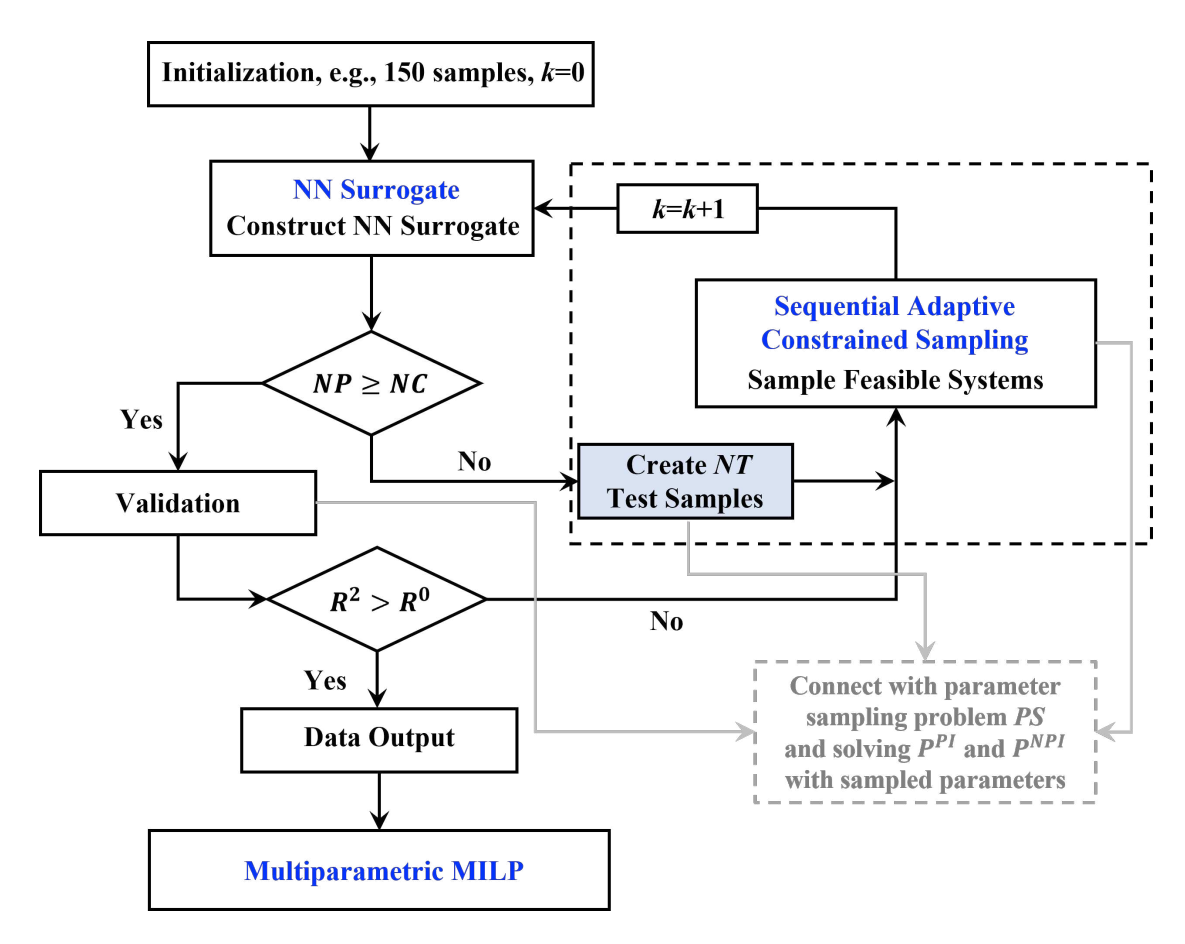


Figure 5: Algorithm flowchart for data-driven multi-parametric programming. The neural network is selected as surrogate to connect input system parameters with output metrics. Adaptive constrained sampling inserts samples at the parametric space with the maximum predicting errors under trained surrogate. The output and validation data are used to train a simpler neural network. This neural network can be reformulated as multi-parametric mixed integer linear programming problem when the neural network activation function is ReLu function.

4.1. Sequential Adaptive Constrained Sampling

The formulation of constrained sampling is adopted from Shachit et al. [37] with constraints from Eqs. 15 – 16 for each sample p. Here, the set $p, p' \in \mathcal{P} = \{1, ..., |\mathcal{P}|\}$ designates the number of samples to evaluate. The set $d, d' \in \mathcal{D} = \{1, ..., |\mathcal{D}|\}$ represents the dimension

of parameter. The detailed formulation (denoted as PS) is given as follows:

 $\min W^2$

s.t.
$$\text{CC-S}_p^{NPI} = f^{NPI}(\tilde{T}_p^{R,NPI}, \tilde{T}_p^{S,NPI}, \tilde{\theta}_{d',p}^{CC})$$
 (21a)

$$(\tilde{x}_{i,p}^{R,NPI}, \tilde{x}_{i,p}^{f,NPI}, \tilde{T}_p^{R,NPI}, \tilde{\theta}_p^{UC}) \in \pi^{\text{NPI-C}}$$

$$(21b)$$

$$CC-S_p^{PI} = f^{PI}(\tilde{T}_p^{R,PI}, \tilde{T}_p^{S,PI}, \tilde{\theta}_{d',p}^{CC})$$
(21c)

$$(\tilde{x}_{i,p}^{R,PI}, \tilde{x}_{i,p}^{f,PI}, \tilde{T}_p^{R,PI}, \tilde{\theta}_p^{UC}) \in \pi^{\text{PI-C}}$$

$$(21d)$$

$$u_{d,p} = \frac{\tilde{\theta}_{d,p} - \theta_d^L}{\theta_d^U - \theta_d^L}, \quad u_{d,p} \in [0,1]$$
(21e)

$$\tilde{\theta}_{d,p} = \{\tilde{\theta}_{d',p}^{CC}, \tilde{\theta}_{p}^{UC}\} \tag{21f}$$

$$W^{2} = \left(\frac{4}{3}\right)^{|D|} + \frac{1}{|\mathcal{P}|^{2}} \sum_{p \in \mathcal{P}} \sum_{p' \in \mathcal{P}} \prod_{d \in D} \left(\frac{3}{2} - |u_{d,p} - u_{d,p'}| + |u_{d,p} - u_{d,p'}|^{2}\right)$$
(21g)

Problem PS generates a series of system parameters which are feasible under both intensified and nonintensified systems. Meanwhile, problem PS is connected with adaptive sampling to improve accuracy of NN surrogate modeling without exhaustively exploring full parametric space [38, 39]. W^2 is the wrap-around L^2 discrepancy (WD) proposed by Hickernell [40]. $u_{d,p}$ is a scaled parameter vector with ranges as [0,1]. Eq. 21e relates the scaled parameter $u_{d,p}$ with original parameters $\tilde{\theta}_{d,p}$. The steps in this section involves the solution of PS to explore the parametric space of $\tilde{\theta}_{d,p} \in \Theta^{n_{\theta} \times |\mathcal{P}|}$. Global optimization of this problem is a challenge when sample size and dimension are large. Next, nonlinear optimization problems mp-NLP^{NPI} and mp-NLP^{PI} are solved respectively to global optimality by fixing property parameters to the solution of PS as $\tilde{\theta}_{d,p}$ for each sample p. Hence the output for NPI system and PI system are maximum driving force respectively. The overall output for given input parameters $\tilde{\theta}_{d,p}$ is the difference of maximum driving force as follows:

$$Y_p = obj^{NPI,*}(\tilde{\theta}_{d,p}) - obj^{PI,*}(\tilde{\theta}_{d,p})$$
(22)

Since input parameter vector θ is scaled as u, a sample p involves a vector of dimensionless system parameters (u) and maximum driving force difference of nonintensified and intensified systems at these parameters (Y_p) .

The problem PS has four uses. Firstly, directly running problem PS yields initial samples. Since the solution of PS is computationally expensive due to nonlinearity and dimensionality, initial samples are generally of small size and obtained using local optimization. Secondly, problem PS is used to generate test samples (with size NT) with random initialization to

identify a parametric vector with maximum prediction errors using neural network surrogate. This test sample is denoted as $S_{p*} = (u_{1,p*}, u_{2,p*}, ..., u_{n^{\theta},p*})$. If we denote the predicted sample output as Y_p^{pred} , then this maximum error identification on sample index is achieved using $p^* = \operatorname{argmax}_p |Y_p - Y_p^{pred}|$.

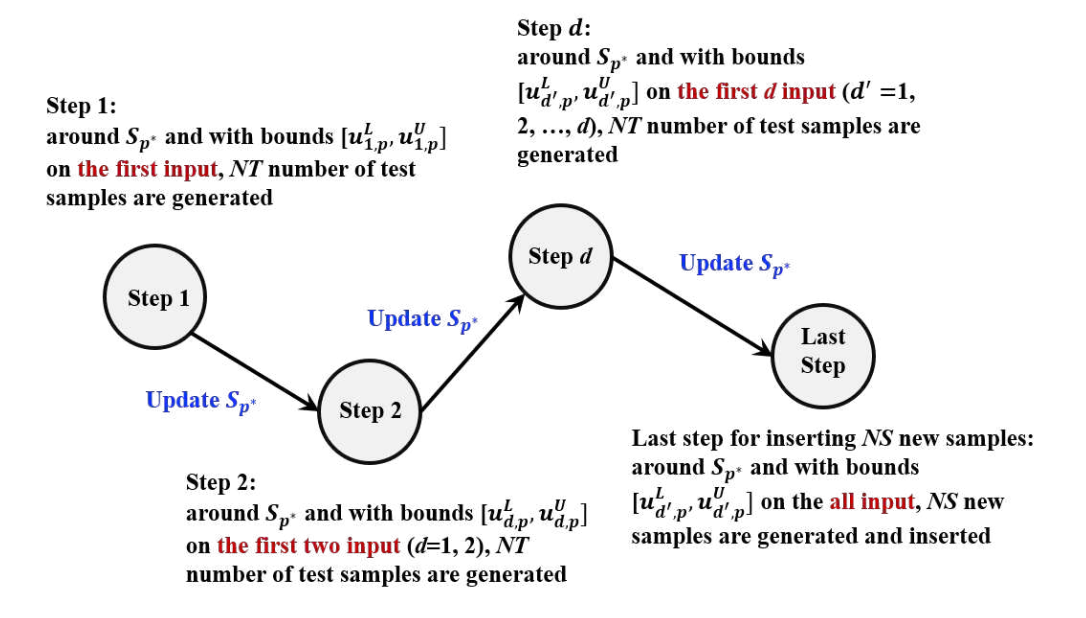


Figure 6: An illustration of sequential adaptive constrained sampling. S_{p*} is the sample with maximum prediction error. S_{p*} is sequentially updated using new test samples, which are generated within sequentially tightened input bounds $[u_{d,p}^L, u_{d,p}^U]$. This procedure improves the identification of data region with maximum prediction errors.

Thirdly, problem PS is used to generate new samples to be added into existing samples. We sequentially create a trust-region on $u_{d,p}$ using a scaling factor σ with a fixed value within range of [0,1]. The trust region is defined as a set of points around the located sample S_{p*} . This procedure is illustrated in Figure 6. The lower and upper bounds of $u_{d,p}$ for this trust-region are $u_{d,p}^L = \sigma u_{d,p^*}$ and $u_{d,p}^U = (2-\sigma)u_{d,p^*}$ respectively ($\sigma = 0.7$ or 0.8). The size of trust region decreases with the increase of σ value. These bounds are sequentially tightened for each $u_{d,p}$ and new test samples are generated accordingly to better locate the region with maximum prediction errors. Within the new bound for $u_{d,p} \in [u_{d,p}^L, u_{d,p}^U]$, problem PS is used to generate some new samples with size NS to insert into the previous sample set. Finally, problem PS is used to generate random samples for validation.

4.2. Multi-parametric Mixed-integer Linear Programming

We use multi-parametric programming to investigate parameters' influence on maximum driving force of nonintensified and intensified systems. The trained neural network with ReLu activation function can be reformulated as a mixed-integer linear programming (MILP) problem [41, 42] and the detailed MILP formulation is given in the Supporting Information. Treating input as varying property parameters, the ReLu neural network can be formulated as a multi-parametric mixed-integer linear programming problem with the following form (mp-MILP^{ReLu}):

$$(\text{mp-MILP}^{ReLu}) \quad \begin{cases} \min & \mu \\ \text{s.t.} & f^{NN}(x,z,u) = 0, \quad g^{NN}(x,z) \leq 0 \\ & \mu \geq 0, \quad x \in X \subseteq R^{n_x}, \quad z \in \{0,1\}^{n_z}, \quad u \in \mathcal{U} \subseteq R^{n_\theta} \end{cases}$$

 μ is a pseudo objective function with lower bound as zero. Hence, mp-MILP^{ReLu} is a parametric feasibility problem with a constant zero objective value. x is the vector of optimization variables in the bounded set $X \subseteq R^{n_x}$. z is the vector of binary variables demonstrating the sign of neuron values, $z = \{Z_{2,1}, Z_{2,2}, ..., Z_{2,|\mathcal{J}|}\}$. u is the vector of continuous 0-1 dimensionless system parameters in the bounded set $\mathcal{U} \subseteq R^{n_\theta}$. For the MILP of trained ReLu neural network, $f^{NN}(x,z,u) = 0$ denotes the linear equalities shown in Eqs. S5a – S5d. Similarly, $g^{NN}(x,z) \leq 0$ are the linear inequalities shown in Eqs. S5e – S5f. The obtained output solution, $x^*(u)$, of mp-MILP^{ReLu} can be expressed as follows [25, 43]:

$$x^{*}(u) = obj^{NPI,*}(\theta) - obj^{PI,*}(\theta) = \begin{cases} h_{1}(u) & \text{if } u \in CR_{1} \\ h_{2}(u) & \text{if } u \in CR_{2} \\ \dots \\ h_{\omega}(u) & \text{if } u \in CR_{\omega} \end{cases}$$

$$(23)$$

Here the optimal objective value $obj^{NPI,*}(\theta)$ and $obj^{PI,*}(\theta)$ are numerically obtained by fixing at sampled property parameters θ . CR_{ω} are unique critical regions for partition w with the expression as $CR_{\omega} = \{u \mid A_{\omega}u \leq B_{\omega}\}$. These critical regions CR_{ω} are polytopes defined as intersection of facets $A_{\omega}u \leq B_{\omega}$ (a set of linear inequalities). The union of these critical regions is the full parametric space, i.e., $\bigcup_{\omega} CR_{\omega} = \mathcal{U}$. The function $h_{\omega}(u)$ is an affine function with the expression as $h_{\omega}(u) = F_{\omega}u + G_{\omega}$. The symbols A_{ω} , B_{ω} , F_{ω} , and G_{ω} are coefficients matrix associated with critical region CR_{ω} . This mp-MILP^{ReLu} problem is solved using MATLAB-based MPT3 toolbox [44].

5. Theoretical Properties

This section summarizes two properties. Property 1 shows that the parametric space of feasible intensified and nonintensified systems can be described as union of CRs. Similarly, Property 2 shows that the parametric space of intensified or nonintensified systems with enhanced driving force can be described as union of CRs.

Property 1. Feasible parametric space of NPI and PI systems is $\bigcup_{\omega} CR_{\omega}$.

Proof. The feasible parameters $u \in \mathcal{U}$ generated using problem PS along with the corresponding output, i.e., Y_p , are connected using ReLu neural network. This ReLu neural network is reformulated as problem mp-MILP^{ReLu}. The solution of the mp-MILP^{ReLu} partitions the input parameter space \mathcal{U} into critical regions CR_{ω} . Hence, $\mathcal{U} = \bigcup_{\omega} CR_{\omega}$.

Property 2. The parametric space of synergistic PI systems is $\bigcup_{\omega} (CR_{\omega} \cap \{h_{\omega}(u) \leq 0\})$.

Proof. The feasible parametric space \mathcal{U} is partitioned into CR_{ω} , i.e., $\mathcal{U} = \bigcup_{\omega} CR_{\omega}$. Within each partition ω , the maximum absolute driving force difference between NPI and PI systems is $x^*(u) = obj^{NPI,*}(\theta) - obj^{PI,*}(\theta) = h_{\omega}(u)$ from Eq. 23.

Eq. 19 gives the condition on when PI is preferred. This is equivalent to $h_{\omega}(u) \leq 0$. Hence, the union of feasibility condition and synergistic condition gives the parametric space of synergistic PI systems, i.e., $\bigcup_{\omega} (CR_{\omega} \cap \{h_{\omega}(u) \leq 0\})$.

Property 2 suggests that the parametric space of synergistic process intensification is the overlapping of reaction-separation feasible space and parametric space with nonpositive maximum diving force between nonintensified and intensified systems. This property also means process intensification does not necessarily lead to enhanced driving force compared with nonintensified counterpart. Note that $\bigcup_{\omega} (CR_{\omega} \cap \{h_{\omega}(u) \leq 0\})$ in Property 2 can be also an empty set if CR_{ω} fully favors nonintensification.

Example. We use a two-parameter example to illustrate Property 1 and Property 2. This example is based on a ternary system (components are M, H, and O) with reaction and vapor-liquid phase equilibrium. The reaction is: $M + H \longleftrightarrow O$. This illustrative example is to find decision boundary transitioning from intensification to nonintensification. The details of this example are discussed in Section 6.3. Constant parameters are summarized in Table 1. Feed composition is $(x_M^0, x_H^0, x_O^0) = (0.48, 0.01, 0.51)$. Varying parameters are slope of phase equilibrium constant for component M, m_M^S , and bubble point, T^{BUB} , with bounds as $\begin{bmatrix} 0.005, 0.015 \end{bmatrix}$ and $\begin{bmatrix} 315 \text{ K}, 335 \text{ K} \end{bmatrix}$ respectively.

Table 1: Fixed parameters for the illustrative example

Feed composition	(x_M^0, x_M^0)	$c_H^0, x_O^0) = (0.48, 0.01)$, 0.51)
Reaction equilibrium		Phase equilibirum	
ΔH^{rxn} for K^R (kJ/kmol)	-7432	m_H^S	0.005
$A_n = lnK^0 \text{ for } K^R$	16.5	m_O^S	0.0016
		b_i^S	0
		T^{DEW} (K)	350

With reference bounds of [0,0.05] and [250 K, 420 K] to scale m_M^S and T^{BUB} , these two scaled parameters are bounded using Eq. 21e as [0.1,0.3] and [0.38,0.5] respectively. The procedure of generating approximate parametric solutions is summarized in Figure 7. For simplicity, we generate input training data on these varying parameters (10,000 data points) using Latincube sampling within bounded two-dimensional space, fix these parameters in mp-NLP^{NPI} and mp-NLP^{PI} and only keep samples which are feasible to both of mp-NLP^{NPI} and mp-NLP^{PI} models. After this step, 4541 samples remain and is shown in Figure 7a. Next, we prepare validation data with smaller size following the same procedure mentioned above and present these data in Figure 7b. The Z-dimension of Figure 7a – b is the difference of maximum driving force between NPI and PI, which is denoted as $100(obj^{NPI,*}(\theta) - obj^{PI,*}(\theta))$. Here, the maximum driving force difference is multiplied with a scaling factor of 100. Note that for both training and validation data, there is a region of infeasibility that are not commonly feasible to NPI and PI models. Furthermore, the red line in Figure 7a indicates an equal driving force of NPI and PI systems and is a decision boundary of intensification and nonintensification.

With training and validation samples, we train a ReLu neural network with 6 neurons and one hidden layer. This trained neural network involves a R^2 of 0.99 and is reformulated as mp-MILP^{ReLu}. This mp-MILP^{ReLu} is solved using MPT3 toolbox with 9 critical regions. Expressions of these critical regions are summarized in Supporting Information. Comparing Figure 7a and Figure 7c, the feasible region of NPI and PI systems are described as union of critical region CR_1 , CR_2 , CR_3 and CR_7 . This validates Property 1. Note that, the feasible region generated using mp-MILP^{ReLu} is expanded into infeasibility region shown Figure 7a. This is because we do not capture the information of sample infeasibility while training neural network. Since only feasible physical samples in a practical system can be obtained in chemical manufacturing, these samples can be still evaluated using the solutions of critical regions or trained neural network to compare driving force differences. Finally, we impose

the condition of preferred PI, as shown in Eq. 19 or 20, on the parametric solutions of mp-MILP^{ReLu}. These relations are essentially cutting planes that divide each critical region into regions of intensification and nonintensification if transition between PI and NPI exists. Specifically, CR_1 fully favors intensification, and division boundary exists in CR_2 , CR_3 and CR_7 for transitioning from intensification to nonintensification. This validates Property 2.

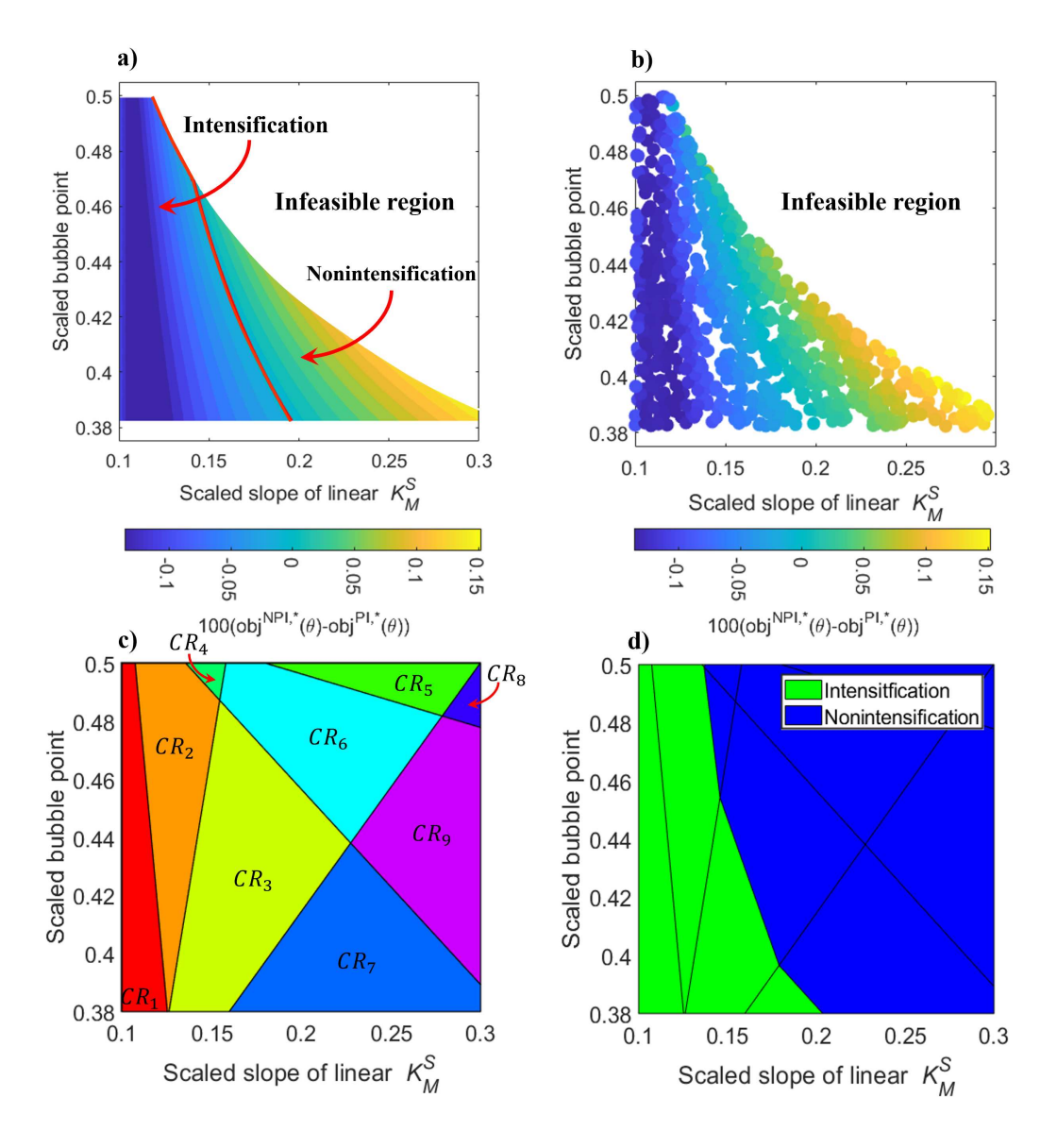


Figure 7: An illustration of parametric properties of intensification and nonintensification. a) Training samples generated from NPI and PI models, b) validation samples generated from NPI and PI models, c) parametric solutions of mp-MILP^{ReLu}, and d) parametric space of NPI and PI. The red line in a) indicates a decision boundary of PI and NPI and is approximated as the boundary of green region and blue region in d). K_M^S is a phase equilibrium constant of component M.

6. Implementation and Case Studies

This section summarizes the implementation of the proposed model and algorithm. The proposed models and algorithms are implemented on reaction-separation systems ranging from methyl acetate production and xylene separation to MTBE production.

6.1. Implementation Details

Unless specified in detailed case studies, the general settings are outlined in this section. Toolbox or software involve toolboxes implemented in MATLAB and optimization software GAMS [45]. MATLAB-based toolboxes include Neural network toolbox [46] for neural network training, Multi-Parameteric Toolbox (MPT3) [44] connected with YALMIP [47] for solving mp-MILP. We also use removeoverlaps function of MPT3 to avoid overlapping of critical regions. Optimization solver in GAMS includes KNITRO [48] and BARON[49]. KNITRO is used for solving problem PS to get samples for initialization, validation and testing or provide initial guess of PS for new samples to be inserted. The size of initial, test and validation samples are 150, 100 and 100 respectively. BARON is used to find sample outputs based on initialization from KNITRO by global optimalization of problem mp-NLP^{PI} and mp-NLP^{NPI} at the sampled parameter θ . The optimization settings for KNITRO are default and BARON is set with maximum CPU time as ten seconds, absolute and relative optimality gap as zero.

We consider a neural network with simple network structure as one input layer, one hidden layer and one output layer. The settings of neural network is default unless mentioned in the specific case study. In the training phase, we use 120 neurons and can use tansig activation function first if poslin activation function does not yield high prediction accuracy. In this way, when test samples are imposed on the current trained prediction models, the parametric space with maximum errors can be better located. If the prediction capability of trained models on the training set is not good enough, the location with maximum errors in the test sample may not be the true location of model errors. Overfitting is avoided due to the random adaptive sampling. After the convergence of adaptive constrained sampling, we retrain a ReLu neural network by reducing the number of neurons using final training samples while not compromising too much prediction accuracy on the validation samples. This helps to reduce the number of binary variables in the mp-MILP^{ReLu}. To reduce computational time, initial test samples and validation samples are prepared using offline parallel computing [50] with random initial starting points by activating random seed in GAMS for solution of problem PS.

6.2. Quaternary Systems with Constant Feed Composition

For reaction-separation systems involving four components, we consider reactions with the form as $A+B\longleftrightarrow C+D$. Components A, B are reactants and components C, D are reaction products. The detailed examples involve methyl acetate production, i.e., methanol (A) + acetic acid $(B) \longleftrightarrow$ methyl acetate (C) + water (D) and m-xylene, p-xylene transmetalation reaction, i.e., sodium p-xylene (A) + m-xylene (B) \longleftrightarrow p-xylene (C) + sodium m-xylene (D). Here, p-xylene and m-xylene are isomers of dimethylbenzene. p-xylene is slightly lighter than m-xylene with their relative volatility as 1.029 and they have close boiling points [51]. For simplicity, m-xylene, sodium p-xylene, sodium m-xylene and p-xylene are denoted as mxy, Napxy, Namxy and pxy respectively. The first reaction produces methyl acetate, which is an effective solvent [52]. The second reaction helps to separate two close-boiling components, i.e., m-xylene and p-xylene, which are industrial solvents or intermediates for many derivatives [53]. The key products of the first and second reaction are methyl acetate and p-xylene respectively.

Table 2: Simplified reaction and phase equilibrium models for four-component systems

Cases	Methyl Acetate production	Transmetalation reaction
Reaction equilibrium	Fitted from Song et al. [54]	Fitted from from Terrill et al. [51]
K^R definition	$K^{R,x} = \frac{x_{MeAc}x_{H2O}}{x_{HOAc}x_{MeOH}}$	$K^{R,x} = rac{x_{Namxy}x_{pxy}}{x_{Napxy}x_{mxy}}$
K^R calculation	$lnK^{R,x} = \frac{-\Delta H}{R} \frac{1}{T} + lnK^0$	$lnK^{R,x} = \frac{-\Delta H}{R} \frac{1}{T} + lnK^0$
$\Delta G^{rxn}/\Delta H^{rxn}$ for K^R	$\Delta H^{rxn} = -1881.82 \text{ kJ/kmol}$	$\Delta H^{rxn} = -3992.88 \text{ kJ/kmol}$
$A_n = lnK^0 \text{ for } K^R$	1	1
Phase equilibrium		
m_A^S	0.0044	0
m_B^S	6×10^{-4}	0.004
m_C^S	0.0105	$1.029 m_B^S$
m_D^S	0.0016	0
T^{BUB} (K)	334.71	413.15
T^{DEW} (K)	359.22	433.15

We first fit the original rigorous reaction model for methyl acetate production [54] and m-xylene, p-xylene transmetalation reaction [51] to composition-based equilibrium reaction model. Phase equilibrium relation of methyl acetate production is fitted from ASPEN HYSYS simulation using UNIQUAC models. Phase equilibrium relation of m-xylene and p-xylene is fitted from equilibrium relation using Antoine equation with ideal gas and ideal

solution approximation while the components Napxy and Namxy are assumed to be non-volatile [51]. Both physical systems are operated under constant pressure of 1 bar. These original models and details of model fitting are given in the Supporting Information. The fitted reaction and phase equilibrium models are summarized in Table 2. $A_n = 1$ as a common fixed reference value for this case study. $b_i^S = 0$ for simplicity of analysis. The reaction temperature range for fitting the first reaction is [313.15 K, 323.15 K] according to the experimental setup in Song et al. [54]. The phase equilibrium temperature range of the first system are [334.5 K, 359.5 K] according to HYSYS simulation. The reaction and phase equilibrium temperature range for fitting the second system are [413.15 K, 433.15 K] according to Terrill et al. [51]

After the data preparation, we compute the general explicit solutions using the proposed data-driven multi-parametric programming. Property parameters are $\theta=(B_1,m_A^S,m_B^S,m_C^S,m_D^S,T^{BUB},T^{DEW})$. The ranges $\left[\theta^L,\theta^U\right]$ for B_1,m_i^S,T^{BUB} and T^{DEW} are $\left[100\text{ K},500\text{ K}\right],\left[0,0.1\right],\left[250\text{ K},420\text{ K}\right]$ and $\left[250\text{ K},500\text{ K}\right]$ respectively. Using these ranges, parameter θ can be scaled to dimensionless parameter $u=\{u_1,u_2,u_3,u_4,u_5,u_6,u_7\}$ with ranges as $\left[0,1\right]$. $u_1,\ u_{2,3,4,5}$ and u_6/u_7 are for $B_1,\ m_i^S,\ T^{BUB}/T^{DEW}$. Besides, $A_n=1$ and $b_i^S=0$ as common fixed reference points. The feed composition for this four-component system is fixed as equal molar feed conditions $x_A^0=x_B^0=0.5$. The prediction performance on maximum driving force difference is given in the Supporting Information with $R^2>0.98$. This neural network is reformulated as mp-MILP ReLu . The parametric solution of this problem for four-component system are summarized in Table S2 – S3 (13 critical regions) of the Supporting Information and encapsulate all single-reaction four-component systems under the simplifying assumptions and given parameter bounds. Any systems with negative maximum driving force difference favors intensification.

Using the fitted data from Table 2, we can find that the dimensionless parametric entry for the methyl acetate production falls into critical region CR_3 with $obj^{NPI,*}(\theta) - obj^{PI,*}(\theta) = -0.569 \times 10^{-2}$. Similarly, dimensionless parametric entry for the system involving transmetalation reaction for the separation of mxy and pxy falls into critical region CR_9 with $obj^{NPI,*}(\theta) - obj^{PI,*}(\theta) = 9.694 \times 10^{-2}$. Hence, the first reaction-separation systems at their given parametric input favors process intensification while the second system favors nonintensification at the given parametric conditions. This prediction can be also validated through direct optimization by running simplified models under these fixed property parameters. The direct optimization for these two systems gives difference of maximum driving force difference as -1.137×10^{-2} (system with reaction 1) and 0.337×10^{-2} (system

with reaction 2) respectively. Decisions of intensification and nonintensification are consistent with predictions. Solution details of these two systems are given in the Section S6 of Supporting Information.

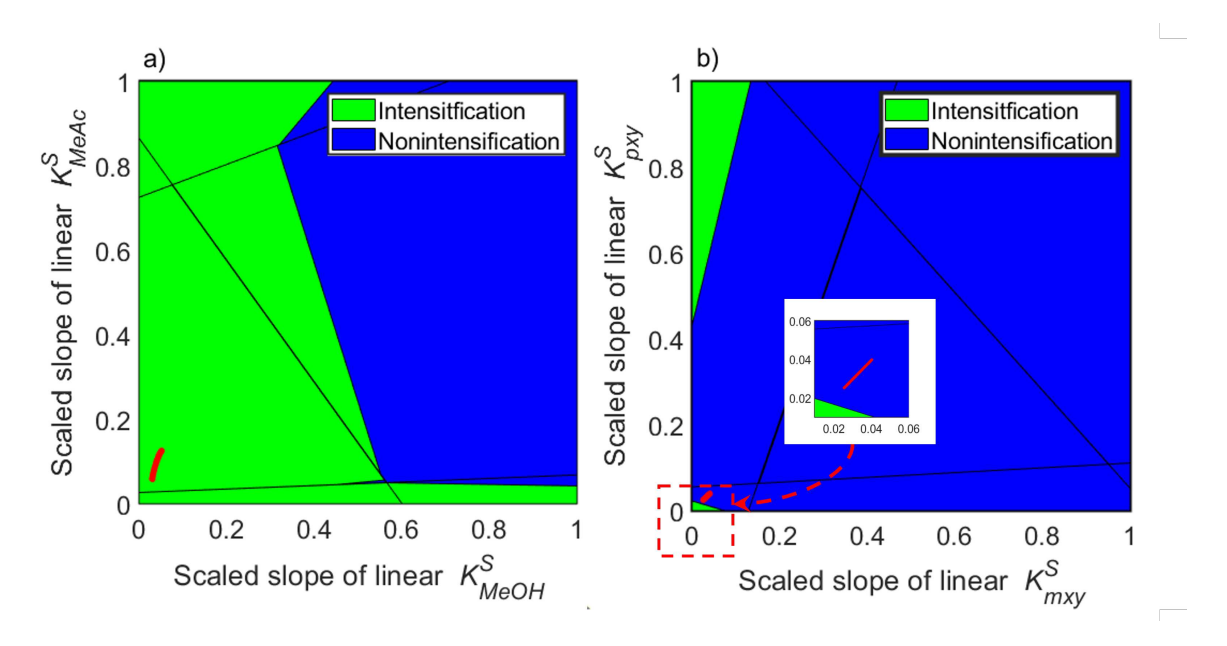


Figure 8: Reduced parametric solutions for four-component system. a) methyl acetate production system, and b) mxy/pxy reaction-separation system. The red lines are operating curve under their corresponding dimensionless phase equilibrium parameters, i.e., u_2 for m_A^S (A is MeOH) and u_4 for m_C^S (C is MeAc) in left figure, u_3 for m_B^S (B is mxy) and u_4 for m_C^S (C is pxy) in right figure.

After investigating PI opportunities for these two cases at the fixed parametric entries, several additional assumptions are imposed to map the parametric solutions of methyl acetate production system and mxy/pxy reaction-separation system into two-dimensional space. This helps to visualize the parametric solutions and study how phase equilibrium property influences synergistic conditions. For methyl acetate production system, these assumptions are :1) the bubble/dew points are $T^{BUB} = 334.71$ K and $T^{DEW} = 359.22$ K according to HYSYS simulation; 2) the slopes for phase equilibrium constant of the first two heaviest component are fixed as constants: $m_B^S = 6 \times 10^{-4}$ for acetic acid and $m_D^S = 0.0016$ for water. Hence the remaining parameters are m_A^S , m_C^S (reaction-related constants are given in Table 2). After scaling for the two fixed values under bounds of $[\theta^L, \theta^U]$, we have $u_1 = 0.316$, $u_3 = 0.006$, $u_5 = 0.016$, $u_6 = 0.498$ and $u_7 = 0.437$. For mxy and pxy reaction-separation system, these assumptions are :1) the bubble/dew points are $T^{BUB} = 413.15K$ and $T^{DEW} = 433.15K$, close to bounds of temperature ranges; 2) the slopes of phase equilib-

rium constant of nonvolatile components are zero, i.e., $m_A^S = m_D^S = 0$. Hence the remaining parameters are m_B^S, m_C^S . After scaling the fixed values, we have $u_1 = 0.951$, $u_2 = u_5 = 0$, $u_6 = 0.960$ and $u_7 = 0.733$. Remaining u_d for these two examples corresponds with slopes of component phase equilibrium constant. Varying remaining u_d for two different systems essentially varies phase equilibrium constant approximation at different temperatures. According to Property 2, the parametric space of synergistic process intensification is the union of feasible space and parametric space with negative maximum driving force difference. Hence after combining the critical expressions in Table S11 – S12 with the constraint $100(obj^{NPI,*}(u) - obj^{PI,*}(u)) \leq 0$ (or ≥ 0), we can get the approximate region involving intensification (or nonintensification). The reduced parametric solutions of methyl acetate production and mxy/pxy reaction-separation systems are shown in Figure 8.

These reduced parametric solutions in Figure 8 show that the hotspot involving synergistic effects are disjoint within the reduced parametric space. By varying temperature within the operating region, the relation between investigated dimensionless phase equilibrium parameters can be obtained from the simulation shown in Figure S3 of Supporting Information. These relations are represented by red lines in Figure 8. The lower and upper ends of these relations correspond with lower and upper bounds of dimensionless equilibrium constant slope m_i^S . As shown in Figure 8, within temperature ranges of phase equilibrium and with equal-ratio feed, mxy/pxy reaction-separation system operate within a very narrow equilibrium constant slope ranges due to their close-boiling mixtures. Furthermore, under equal molar feed composition, methyl acetate production system always favors intensification and mxy/pxy reaction-separation system always favor nonintensification.

6.3. Ternary Systems with Varying Feed Composition

The ternary systems involve reactions with the form as $M + H \longleftrightarrow O$. Components M, H are reactants and O is the desired product. This case study shows how synergistic effects evolve with feed compositions. Specifically, we consider a reaction for MTBE production, i.e., isobutene (M) + methanol $(H) \longleftrightarrow \text{MTBE}(O)$. The investigated reaction is significant in chemical industry. For instance, the reaction product MTBE can be used as fuel additive or solvent [55]. Although the reference parameters are based on MTBE production, additional reaction and separation systems are included if their property parameters fall into investigated parameter bounds. Simulation and simplified reaction/phase equilibrium models are given in Figure S6 and Table S5 of Supporting Information.

To reduce computational efforts, three most important composition points are considered

at the approximate region of extreme driving force reported in Lopez-Arenas et al. [21]. These composition points are $(x_{i-butene}^0, x_{MeOH}^0, x_{MTBE}^0) = (0.05, 0.8, 0.15)$ (composition I), (0.2, 0.2, 0.6) (composition II), and (0.48, 0.01, 0.51) (composition III). Composition I and III correspond with maximum driving force while composition II correspond with minimum driving force [21]. These compositions represent compositions in typical MTBE reactive distillation stages [56]. For example, composition III (rich in isobutene and MTBE) appears above isobutene feed stage, composition II is located at bottom of column (rich in MTBE) and composition I (rich in methanol) appears below methanol feed stage.

Table 3: Fixed and varying parameters for system projections

	MTBE production		
Cases	Composition I	Composition II	Composition III
Reaction equilibrium			
ΔH^{rxn} for K^R (kJ/kmol)	-7166.9	-7275.2	-7432
$A_n = lnK^0 \text{ for } K^R$	16.5	16.5	16.5
Phase equilibrium			
m_O^S	0.0029	0.0014	0.0008
T^{BUB} (K)	364.3	381	320
T^{DEW} (K)	424.0	399.5	371.5

The involved property parameters are $\theta = (B_1, m_M^S, m_H^S, m_O^S, T^{BUB}, T^{DEW})$. The bounds $[\theta^L, \theta^U]$ for B_1, m_i^S, T^{BUB} and T^{DEW} are [100 K, 500 K], [0, 0.05], [250 K, 420 K] and [250 K, 500 K] respectively. Using these ranges, parameter θ can be scaled to 0-1 dimensionless parameter $u = \{u_1, u_2, u_3, u_4, u_5, u_6\}$. $u_1, u_{2,3,4}$ and u_5/u_6 are for $B_1, m_i^S, T^{BUB}/T^{DEW}$. Besides, $A_n = 16.5$ and $b_i^S = 0$ as common fixed reference points. The prediction performance $(R^2 \geq 0.98)$ and parametric solutions of ternary system are given in Section S7 of Supporting Information. Several additional assumptions are imposed to map the parametric solutions of ternary systems into two-dimensional space. The fixed parameters involve the reaction-related constants (B_1) and bubble/dew points (T^{BUB}/T^{DEW}) , the slopes for phase equilibrium constant of product $O(m_O^S)$. The varying parameters are slopes for phase equilibrium constant of two reactants (m_M^S, m_H^S) . Since some property parameters are fixed for projection, states (composition and temperature) at these fixed values may not be achieved. Hence not all random combinations of these fixed property parameters ensure the feasibility of mp-NLP^{NPI} and mp-NLP^{PI}. To ensure the feasibility of simplified models, we run constrained sampling problem PS to obtain these property parameters to

be fixed, which are close to property parameters obtained from HYSYS simulation (Table S5). Then, using these fixed property parameters, all samples for the varying parameters (m_M^S, m_H^S) are feasible. The final fixed parameters are summarized in Table 3.

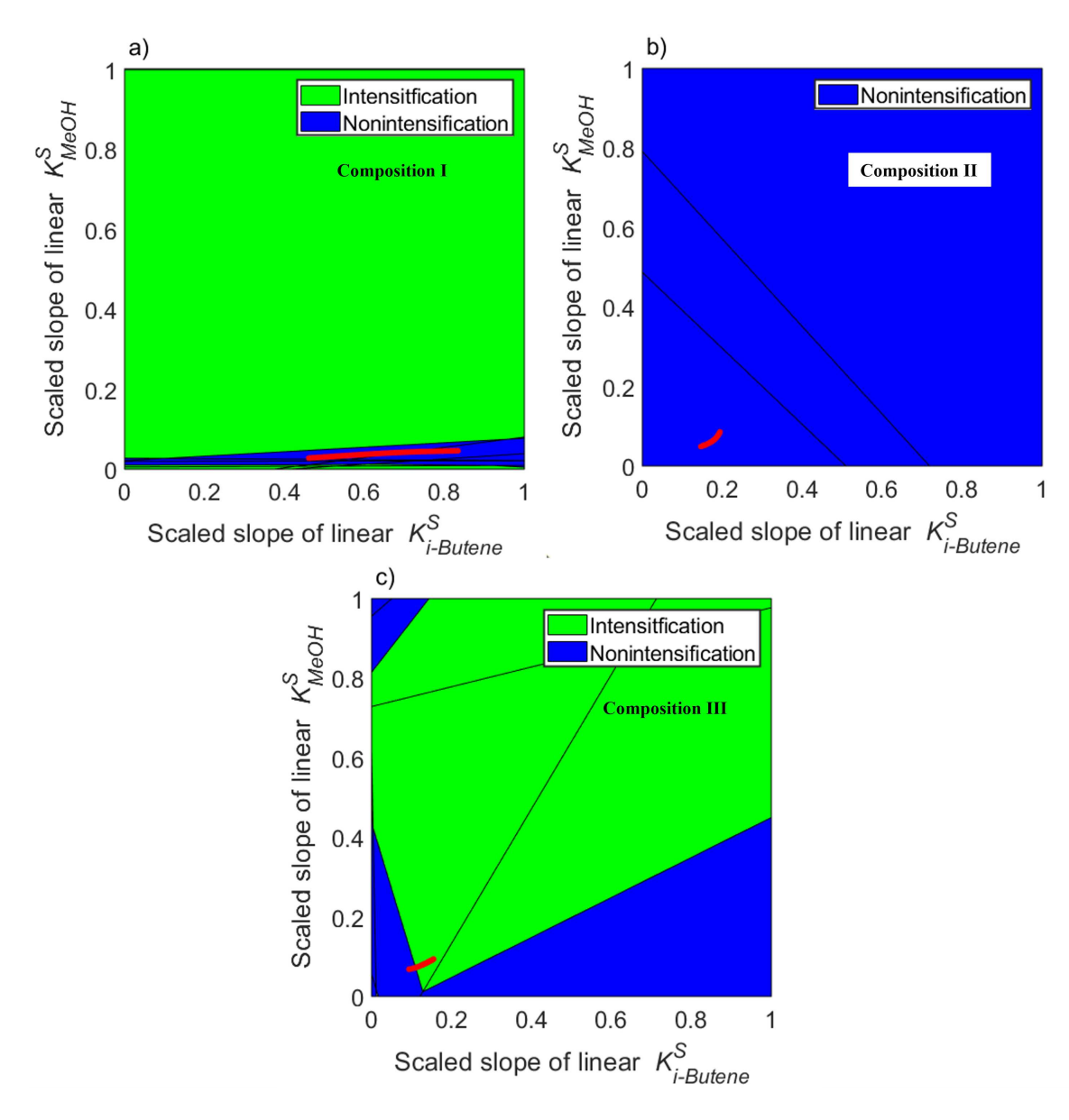


Figure 9: Reduced parametric solutions for three-component system. a) Feed composition I, b) Feed composition II, and c) Feed composition III. The red lines are dimensionless property parameters of phase equilibrium constants, i.e., u_2 for m_M^S (M is i-butene) and u_3 for m_H^S (H is methanol).

According to Property 2, the parametric space of synergistic process intensification is the union of feasible space and parametric space with negative maximum driving force difference.

Hence after combining the critical region expressions with the constraint $100(obj^{NPI,*}(u) - obj^{PI,*}(u)) \leq 0$ (or ≥ 0), we obtain the approximate region involving intensification (or non-intensification). The reduced parametric solutions of ternary systems are given in Figure 9. The sampled property parameters (m_M^S, m_H^S) through constrained adaptive sampling are marked as red lines on system parametric solutions. At composition I and II and within investigated parametric domains, the ternary system always favor nonintensification. At composition III, most of operating region stay within region of intensification. However, narrow region of transitioning from nonintensification to intensification exists, which suggests equal maximum driving force at transition boundary.

To explain the transition from NPI to PI, sensitivity analysis is implemented at sampled m_M^S and m_H^S values. m_M^S/m_H^S is recalculated as relative volatility using Eq. 14 (note $b_i^S = 0$). The sensitivity analysis is shown in Figure 10. At lower relative volatility, phase equilibrium temperature is high since separation is more difficult (Figure 10d). Reaction temperature in nonintensified system can be lower than that of intensified system due to decoupling of reaction and phase equilibrium temperature. In fact, nonintensified system reaction temperature is always at the temperature lower bound 250 K if sufficient amount of cooling utility is supplied. Since the reaction is exothermic, reaction yield of product O is higher in nonintensified system than intensified system (Figure 10e). Product O is the heaviest component at composition III and hence more product O remains in liquid phase for nonintensified system (Figure 10b). This results in a favorable region of nonintensification in Figure 9c. As the temperature increases, the effect of product removing into vapor phase through phase equilibrium is enhanced. This product removing effect facilitates reaction yield in intensification system (Figure 10e) and hence results in higher absolute driving force. Then production of product O using intensified system is more favorable at higher relative volatility. This critical relative volatility is 1.47 when PI outperforms NPI (Figure 10c). If relative volatility further increases, separation becomes easier and lower separation temperature is required to achieve maximum driving force. When separation temperature decreases to bubble point, few vapor flow exists and system involves weak physical meaning.

To summarize, this analysis demonstrates the competing phenomena and synergistic effects between reaction and phase equilibrium. Besides, this suggests the existence of critical property region with favorable transition from nonintensification to intensification or vice versa. Furthermore, it shows that the proposed data-driven parametric programming algorithm facilitates the identification of intensification hot-spots with physical interpretation.

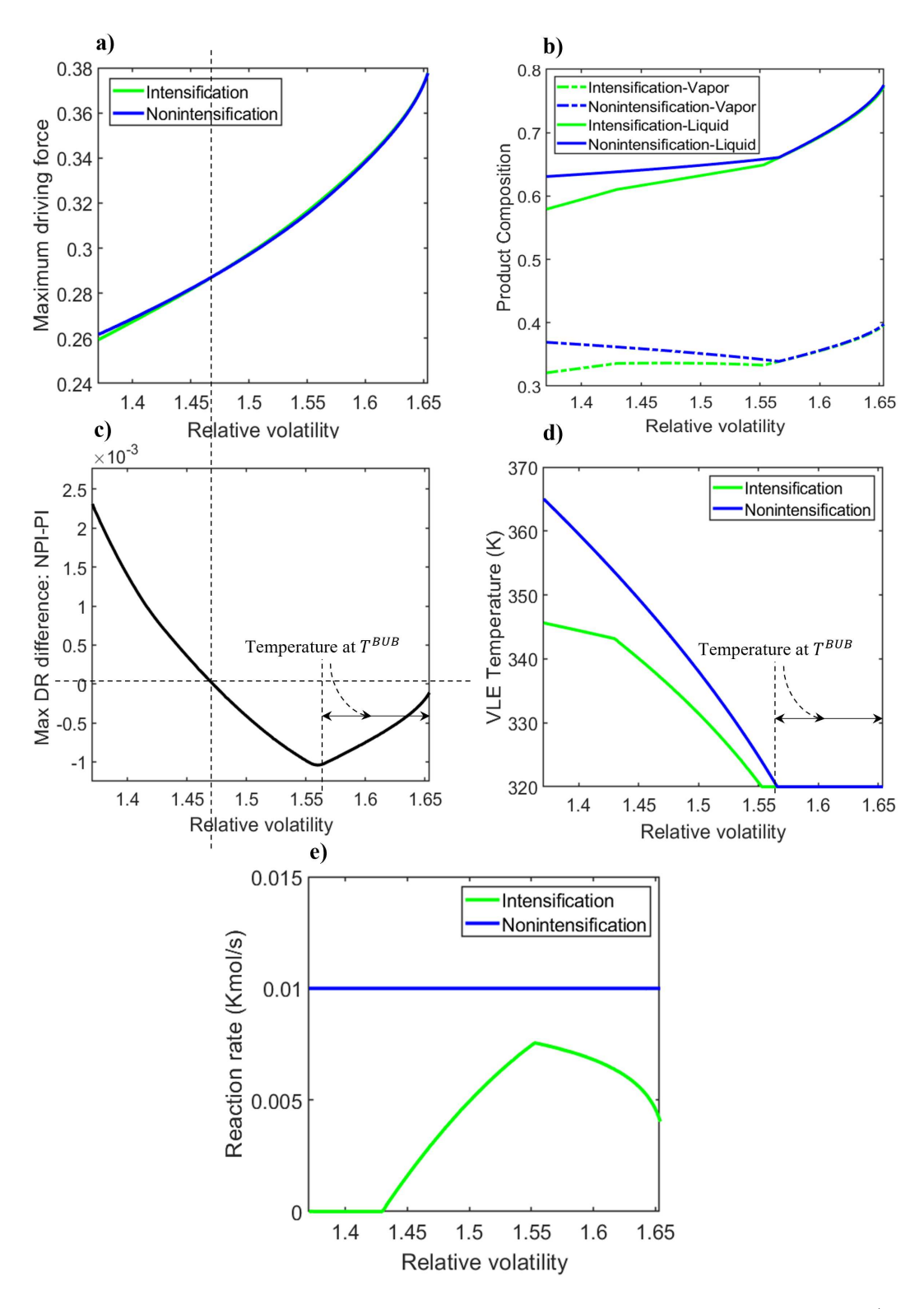


Figure 10: Change of objective function and decisions with relative volatility at composition III. a) Maximum driving force objective, b) Decisions of phase equilibrium product compositions, c) Driving force difference between NPI and PI, d) Decisions of phase equilibrium temperature and e) Decisions of reaction rate. Critical relative volatility exists with favorable transition from NPI to PI systems.

7. Conclusions

Given design targets and component property parameters, understanding synergistic domains of process intensification is critical for decision making of intensified (PI) or nonintensified (NPI) systems. In this work, we approximate the synergistic domains through data-driven parametric programming based on solutions of PI and NPI system models. These models leverage common model building blocks with unique conditions for intensified and nonintensified systems. Simplifying assumptions, i.e., composition-based reaction equilibrium constant and approximate linear phase equilibrium relations, are imposed to reduce number of system parameters. Hence, models of intensfied and nonintensified systems are mp-NLP with parameters defining reaction and separation. We refer synergistic domains as ranges of system parameters with enhanced maximum driving force for intensified systems. These ranges are identified using an algorithm of data-driven multi-parametric programming by reformulating ReLu neural network surrogate as mp-MILP. We show feasibility conditions of nonintensifed and intensfied systems can be represented as union of critical regions. Similarly, we represent synergistic domains with PI outperforming NPI using critical regions. The proposed framework is applied to multi-component reaction-separation systems. With equal-mole feed conditions of reactants, the methyl acetate production system always favor intensification while m-xylene/p-xylene production system always favors nonintensification. By varying ternary system feed composition, we show that at composition region rich in more volatile reactant and least volatile product, the transition from nonintensification to intensification happen at critical reactant relative volatility. Future work involves the application of these synergistic conditions for process design, and bounding process synthesis and intensification.

Acknowledgment

The authors gratefully acknowledge funding support from the NSF CAREER award CBET-1943479, and the DOE RAPID Institute SYNOPSIS Project (DE-EE0007888-09-03). Jianping Li appreciates the Brunner Barns Fellowship awarded by Texas A&M University Artie McFerrin Department of Chemical Engineering. Part of the research was conducted with computing resources provided by Texas A&M High Performance Research Computing.

References

[1] S. E. Demirel, J. Li, M. F. Hasan, Systematic process intensification using building blocks, Computers & Chemical Engineering 105 (2017) 2–38.

- [2] J. Bielenberg, I. Palou-Rivera, The rapid manufacturing institute—reenergizing us efforts in process intensification and modular chemical processing, Chemical Engineering and Processing-Process Intensification 138 (2019) 49–54.
- [3] A. K. Tula, M. R. Eden, R. Gani, Computer-aided process intensification: Challenges, trends and opportunities, AIChE Journal 66 (1) (2019).
- [4] S. E. Demirel, J. Li, M. F. Hasan, Systematic process intensification, Current Opinion in Chemical Engineering 25 (2019) 108–113.
- [5] T. Van Gerven, A. Stankiewicz, Structure, energy, synergy, time the fundamentals of process intensification, Industrial & engineering chemistry research 48 (5) (2009) 2465–2474.
- [6] K. Huang, S.-J. Wang, L. Shan, Q. Zhu, J. Qian, Seeking synergistic effect—a key principle in process intensification, Separation and purification technology 57 (1) (2007) 111–120.
- [7] N. J. Sucher, Searching for synergy in silico, in vitro and in vivo, Synergy 1 (1) (2014) 30–43.
- [8] J. C. Carrasco, F. V. Lima, Novel operability-based approach for process design and intensification: Application to a membrane reactor for direct methane aromatization, AIChE Journal 63 (3) (2017) 975–983.
- [9] M. S. Monjur, S. E. Demirel, J. Li, M. F. Hasan, Spice_mars: A process synthesis framework for membrane-assisted reactive separations, Industrial & Engineering Chemistry Research 60 (20) (2021) 7635-7655.
- [10] J. Li, S. E. Demirel, M. F. Hasan, Systematic process intensification involving zeotropic distillation, In: Computer Aided Chemical Engineering 47 (2019) 421–426.
- [11] A. K. Tula, B. Befort, N. Garg, K. V. Camarda, R. Gani, Sustainable process design & analysis of hybrid separations, Computers & Chemical Engineering 105 (2017) 96–104.
- [12] J. Li, S. E. Demirel, M. F. Hasan, Process integration using block superstructure, Industrial & Engineering Chemistry Research 57 (12) (2018) 4377–4398.
- [13] W. R. Huster, A. M. Schweidtmann, J. T. Lüthje, A. Mitsos, Deterministic global superstructure-based optimization of an organic rankine cycle, Computers & Chemical Engineering 141 (2020) 106996.
- [14] H. Yu, C. Fu, T. Gundersen, Work exchange networks (wens) and work and heat exchange networks (whens): A review of the current state of the art, Industrial & Engineering Chemistry Research 59 (2) (2019) 507–525.
- [15] A. A. Kiss, M. Jobson, X. Gao, Reactive distillation: stepping up to the next level of process intensification, Industrial & Engineering Chemistry Research 58 (15) (2018) 5909–5918.

- [16] S. E. Demirel, J. Li, M. F. Hasan, A general framework for process synthesis, integration and intensification, in: Computer Aided Chemical Engineering, Vol. 44, Elsevier, 2018, pp. 445–450.
- [17] C. Wang, Y. Zhuang, L. Liu, L. Zhang, J. Du, Design and comparison of energy-saving double column and triple column reactive-extractive hybrid distillation processes for ternary multi-azeotrope dehydration, Separation and Purification Technology 259 (2021) 118211.
- [18] V. Agreda, W. Heise, High-purity methyl acetate via reactive distillation, Chemical Engineering Progress 86 (2) (1990) 40–46.
- [19] J. J. Siirola, Industrial applications of chemical process synthesis, in: Advances in chemical engineering, Vol. 23, Elsevier, 1996, pp. 1–62.
- [20] J. Li, S. E. Demirel, M. F. Hasan, Process synthesis using block superstructure with automated flowsheet generation and optimization, AIChE Journal 64 (8) (2018) 3082–3100.
- [21] T. Lopez-Arenas, M. Sales-Cruz, R. Gani, E. S. Pérez-Cisneros, Thermodynamic analysis of the driving force approach: Reactive systems, Computers & Chemical Engineering 129 (2019) 106509.
- [22] Y. Tian, E. N. Pistikopoulos, Toward an envelope of design solutions for combined/intensified reaction/separation systems, Industrial & Engineering Chemistry Research 59 (24) (2020) 11350–11354.
- [23] S. E. Demirel, J. Li, M. El-Halwagi, M. F. Hasan, Sustainable process intensification using building blocks, ACS Sustainable Chemistry & Engineering 8 (48) (2020) 17664–17679.
- [24] E. N. Pistikopoulos, L. Dominguez, C. Panos, K. Kouramas, A. Chinchuluun, Theoretical and algorithmic advances in multi-parametric programming and control, Computational Management Science 9 (2) (2012) 183–203.
- [25] V. M. Charitopoulos, Uncertainty-aware integration of control with process operations and multiparametric programming under global uncertainty, Springer Nature, 2020.
- [26] Z. Li, M. G. Ierapetritou, Process scheduling under uncertainty using multiparametric programming, AIChE journal 53 (12) (2007) 3183–3203.
- [27] M. M. Papathanasiou, F. Steinebach, M. Morbidelli, A. Mantalaris, E. N. Pistikopoulos, Intelligent, model-based control towards the intensification of downstream processes, Computers & Chemical Engineering 105 (2017) 173–184.
- [28] R. Oberdieck, E. N. Pistikopoulos, Multi-objective optimization with convex quadratic cost functions: A multi-parametric programming approach, Computers & Chemical Engineering 85 (2016) 36–39.
- [29] R. Oberdieck, N. A. Diangelakis, M. M. Papathanasiou, I. Nascu, E. N. Pistikopoulos, Pop-parametric optimization toolbox, Industrial & Engineering Chemistry Research 55 (33) (2016) 8979–8991.

- [30] M. Wittmann-Hohlbein, E. N. Pistikopoulos, On the global solution of multi-parametric mixed integer linear programming problems, Journal of Global Optimization 57 (1) (2013) 51–73.
- [31] J. D. Seader, E. J. Henley, D. K. Roper, Separation process principles, Vol. 25, wiley New York, 1998.
- [32] W. D. Seider, J. D. Seader, D. R. Lewin, Product & Process Design Principles: Synthesis, Analysis and Evaluation, John Wiley & Sons, 2009.
- [33] J. Li, Methods and Algorithms for Process Synthesis and Intensification using Building Blocks, Texas A&M University, 2020.
- [34] R. V. Sanderson, H. Chien, Simultaneous chemical and phase equilibrium calculation, Industrial & Engineering Chemistry Process Design and Development 12 (1) (1973) 81–85.
- [35] D. Barbosa, M. F. Doherty, The influence of equilibrium chemical reactions on vapor—liquid phase diagrams, Chemical Engineering Science 43 (3) (1988) 529–540.
- [36] L. T. Biegler, I. E. Grossmann, A. W. Westerberg, Systematic methods for chemical process design (1997).
- [37] S. S. Iyer, I. Bajaj, P. Balasubramanian, M. F. Hasan, Integrated carbon capture and conversion to produce syngas: novel process design, intensification, and optimization, Industrial & Engineering Chemistry Research 56 (30) (2017) 8622–8648.
- [38] A. Bhosekar, M. Ierapetritou, Advances in surrogate based modeling, feasibility analysis, and optimization: A review, Computers & Chemical Engineering 108 (2018) 250–267.
- [39] L. Dias, A. Bhosekar, M. Ierapetritou, Adaptive sampling approaches for surrogate-based optimization, in: Computer Aided Chemical Engineering, Vol. 47, Elsevier, 2019, pp. 377–384.
- [40] F. J. Hickernell, Lattice rules: how well do they measure up?, In: Random and quasi-random point sets (1998) 109–166.
- [41] B. Grimstad, H. Andersson, ReLU networks as surrogate models in mixed-integer linear programs, Computers & Chemical Engineering 131 (2019) 106580.
- [42] C. Tsay, J. Kronqvist, A. Thebelt, R. Misener, Partition-based formulations for mixed-integer optimization of trained relu neural networks, Advances in Neural Information Processing Systems 34 (2021) 3068–3080.
- [43] S. Avraamidou, Mixed-integer multi-level optimization through multi-parametric programming, Imperial College London, 2018.
- [44] M. Herceg, M. Kvasnica, C. N. Jones, M. Morari, Multi-parametric toolbox 3.0, in: 2013 European control conference (ECC), IEEE, 2013, pp. 502–510.

- [45] M. R. Bussieck, A. Meeraus, General algebraic modeling system (gams), In: Modeling languages in mathematical optimization (2004) 137–157.
- [46] M. H. Beale, M. T. Hagan, H. B. Demuth, Neural network toolbox, User's Guide, MathWorks 2 (2010) 77–81.
- [47] J. Lofberg, Yalmip: A toolbox for modeling and optimization in matlab, in: 2004 IEEE international conference on robotics and automation (IEEE Cat. No. 04CH37508), IEEE, 2004, pp. 284–289.
- [48] J. Nocedal, Knitro: an integrated package for nonlinear optimization, In: Large-Scale Nonlinear Optimization (2006) 35–60.
- [49] N. V. Sahinidis, Baron: A general purpose global optimization software package, Journal of global optimization 8 (2) (1996) 201–205.
- [50] J. Palach, Parallel programming with Python, Packt Publishing Ltd, 2014.
- [51] D. L. Terrill, L. F. Sylvestre, M. F. Doherty, Separation of closely boiling mixtures by reactive distillation. 1. theory, Industrial & Engineering Chemistry Process Design and Development 24 (4) (1985) 1062–1071.
- [52] B. T. F. de Mello, I. J. Iwassa, R. P. Cuco, V. A. dos Santos Garcia, C. da Silva, Methyl acetate as solvent in pressurized liquid extraction of crambe seed oil, The Journal of Supercritical Fluids 145 (2019) 66–73.
- [53] Y. F. Yeong, A. Z. Abdullah, A. L. Ahmad, S. Bhatia, Process optimization studies of p-xylene separation from binary xylene mixture over silicalite-1 membrane using response surface methodology, Journal of Membrane Science 341 (1-2) (2009) 96–108.
- [54] W. Song, G. Venimadhavan, J. M. Manning, M. F. Malone, M. F. Doherty, Measurement of residue curve maps and heterogeneous kinetics in methyl acetate synthesis, Industrial & engineering chemistry research 37 (5) (1998) 1917–1928.
- [55] S. Sridhar, B. Smitha, A. Shaik, Pervaporation-based separation of methanol/mtbe mixtures—a review, Separation and Purification Reviews 34 (1) (2005) 1–33.
- [56] R. Jacobs, R. Krishna, Multiple solutions in reactive distillation for methyl tert-butyl ether synthesis, Industrial & Engineering Chemistry Research 32 (8) (1993) 1706–1709.